International Core Journal of Engineering Volume 12 Issue 11, 2026
ISSN: 2414-1895 DOI: 10.6919/ICJE.202611_12(11).0012

Extraction of Friction Coefficient for Spline Tooth Surfaces based on MB Fractal Contact Model and Ultra-Depth-of-Field Topography

Tenglang Luo, Jinsheng Liang, Min Zhang

College of Mechanical and Electrical Engineering, Shaanxi University of Science and Technology, Xi'an 710021, Shaanxi, China

Abstract

In the dynamic modeling of spline rotors, the friction coefficient is often assigned a fixed empirical value, which fails to reflect the regulatory effect of microscopic tooth surface morphology on friction behavior. To address this issue, this paper relies on the Majumdar-Bhushan (MB) fractal contact theory, incorporating the adhesion effect and plowing effect into a unified framework to establish a quantitative mapping relationship between the friction coefficient and the tooth surface fractal characteristic parameters (fractal dimension D, scale coefficient G). With the aid of an ultra-depth-of-field optical microscope, three-dimensional topography was collected from 6 tooth surface regions of three sets of spline specimens from the same batch. From these, 18 one-dimensional profile curves were intercepted, and the fractal dimension and scale coefficient were calculated individually using the power spectrum method, which were then substituted into the model for numerical solution of the equivalent friction coefficient. The results show that the tooth surface roughness Ra ranges from 1.106 to 4.471 μm, the fractal dimension D ranges from 1.234 to 1.643, and Roughness peak G* ranges from 5.783×10^{-6} to 1.150×10^{-5}. The calculated friction coefficient μ falls within the range of 0.07 to 0.25, which is highly consistent with the empirical range for ground tooth surfaces (0.05 to 0.3). The above work provides a pathway for determining the friction coefficient that accounts for surface topography effects for spline rotor dynamic models, effectively avoiding the blindness of empirical value assignment.

Keywords

Spline Rotor; MB Fractal Contact Model; Friction Coefficient; Surface Topography; Power Spectrum Method; Ultra-Depth-Of-Field Microscopy.

1. Introduction

Spline connection structures, owing to their advantages of high load-carrying capacity, high centering accuracy, and flexible axial sliding, have been widely applied in the rotor systems of high-speed rotating machinery such as aero-engines and gas turbines [1-3]. During service, spline pairs are subjected to complex alternating loads, and the microscopic slip behavior and energy dissipation mechanism of the tooth surfaces are largely governed by the friction coefficient, which in turn exerts a profound influence on the dynamic characteristics of the spline rotor system.

The role of the friction coefficient in the spline rotor system can be understood from three aspects. First, the friction coefficient directly participates in regulating the nonlinear stiffness and damping characteristics of the spline element. Slip friction on the tooth surfaces induces pronounced nonlinear behavior, and the energy dissipation rate in the slip region increases accordingly, causing the friction surfaces to exhibit a "friction hardening" phenomenon. Second, the distribution pattern of the contact

ISSN: 2414-1895 DOI: 10.6919/ICJE.202611_12(11).0012

stress on the tooth surfaces is constrained by the friction state; when the friction coefficient is relatively high, the stress concentration at the tooth-root transition curve is significantly amplified, and the rated service life of the spline is thereby substantially reduced. Third, the friction coefficient plays a decisive role in the instability threshold of the rotor system in the supercritical speed region. Classical rotor dynamics theory indicates that self-excited vibration induced by internal damping or dry friction originates from the energy input to the system through the work done by tangential forces during rotor whirling; once the input energy exceeds the energy dissipated by the system damping, the system enters an unstable state. Under high-speed operating conditions, even a slight perturbation of the friction coefficient can cause a significant shift in the instability speed of the system.

In traditional rotor dynamics models, the friction coefficient is often taken as a fixed empirical constant, which cannot reflect the differences in tooth-surface friction behavior under different machining processes and different surface conditions. The real contact of rough surfaces occurs at the microscopic scale, and its contact behavior is closely related to the statistical characteristics of surface topography. The MB contact model proposed by Majumdar and Bhushan on the basis of fractal geometry theory [4] employs two parameters, the fractal dimension D and the scale coefficient G, to describe the multi-scale self-similar characteristics of rough surfaces. This model breaks through the dependence of traditional statistical methods on sampling length and instrument resolution, and is capable of describing contact behavior uniformly from the microscopic to the macroscopic scale.

At present, reports on applying the MB fractal contact theory to the study of the friction characteristics of transmission components such as gears and splines remain scarce, and most studies adopt standard roughness parameters or assumed fractal parameters, lacking parameter extraction and friction coefficient inversion based on actual tooth-surface topography observations. In view of this, the following work is carried out in this paper:

(1) Based on the MB fractal contact theory, and incorporating the adhesion and plowing effects, an analytical model is established between the friction coefficient and the fractal parameters of the tooth surface;

(2) An ultra-depth-of-field optical microscope is used to observe the three-dimensional topography of the tooth surfaces of spline specimens, one-dimensional profile curves are intercepted, and the fractal dimension and scale coefficient are extracted by means of the power spectrum method;

(3) Through the numerical solution of 18 profile curves from three sets of parallel specimens, the equivalent friction coefficient of the spline tooth surface is extracted, and the rationality of the model is verified by comparison with traditional empirical values.

2. Theoretical Model

2.1 MB Fractal Contact Model

The MB (Majumdar-Bhushan) contact model based on fractal geometry theory breaks through the limitations of traditional statistical methods (such as the Gaussian distribution assumption). It no longer relies on measurement results of sampling length and instrument resolution, but rather describes the contact behavior of rough surfaces uniformly from microscopic to macroscopic scales based on the essential characteristic of statistical self-similarity of surfaces. The core of the MB fractal contact model lies in using two independent parameters, the fractal dimension and the scale coefficient, to reflect the complexity of surface roughness, the space-filling capacity, and the amplitude characteristics of the surface, thereby constructing a functional relationship between the contact load P and the contact area Ar, which is specifically expanded as follows [4-7]:

First, consider the contact behavior of two contacting surfaces at different stages. Assuming the contact area of an asperity is a, there exists a critical boundary between the elastic and plastic regions, denoted as the critical contact area a_c. When $a < a_c$, plastic deformation occurs; whereas when $a > a_c$, elastic deformation occurs. The expression for the critical contact area a_c is given in Eq.(1):

ISSN: 2414-1895 DOI: 10.6919/ICJE.202611_12(11).0012

$$a_c = G^2 / \left(\frac{K\phi}{2} \right)^{\frac{2}{D-1}} \tag{1}$$

In the equation, G is the scale coefficient, K is the correlation coefficient between the hardness H and the yield strength σ_y (H=K/σ_y), and $\phi = \sigma_y / E$ is a characteristic parameter of the material. E is the composite elastic modulus (1/E = (1-\$\nu_1^2$)/E1 + (1-\$\nu_2^2$)/E2), where E_i and ν_i are the elastic moduli and Poisson's ratios of the two contacting surfaces, respectively; D is the fractal dimension.

The total contact area of the two contacting surfaces comprises two parts: the elastic contact area A_{re} and the plastic contact area A_{rp}. Calculation is divided into the following two cases based on the maximum asperity contact area al and the critical contact area ac.

When $a_l > a_c$:

$$\begin{cases} A_{re} = \dfrac{D}{2-D}[a_l^{D/2} - a_l^{D/2} a_c^{(2-D)/2}] \\ A_{rp} = \dfrac{D}{2-D} a_l^{D/2} a_c^{(2-D)/2} \end{cases} \tag{2}$$

When $a_l < a_c$:

$$\begin{cases} A_{re} = 0 \\ A_{rp} = \dfrac{D}{2-D} a_l \end{cases} \tag{3}$$

The total contact area A_r is given by:

$$A_r = A_{re} + A_{rp} \tag{4}$$

According to the different ranges of the fractal dimension D and the relationship between the maximum asperity contact area al and the critical contact area a_c, the calculation formula for the contact load P is as follows (expressed in terms of the dimensionless load P^*):

When $a_l > a_c$, both elastic and plastic deformations occur on the rough surface.

For $1<D<2$ and $D \neq 1.5$:

$$P^* = \frac{4\sqrt{\pi} G^{*D-1}}{3} g_1(D) A_r^{*\frac{D}{2}} \left\{ \left[\frac{(D-2)A_r^*}{D} \right]^{(3-2D)/2} - a_c^{*(3-2D)/2} \right\} + K\phi g_2(D) A_r^{*D/2} a_c^{*(3-2D)/2} \tag{5}$$

where $g_1(D) = \dfrac{D}{3-2D}\left(\dfrac{2-D}{D}\right)^{D/2}$, $g_2(D) = \left(\dfrac{D}{2-D}\right)^{1-D/2}$, $P^* = \dfrac{P}{A_a E}$, $G^* = \dfrac{G}{\sqrt{A_a}}$,

$A_r^* = \dfrac{A_r}{A_a}$, $a_c^* = \dfrac{a_c}{A_a}$, and A_a is the nominal contact area.

ISSN: 2414-1895 DOI: 10.6919/ICJE.202611_12(11).0012

For D=1.5:

$$P^* = \sqrt{\pi} G^{*(1/2)} \left(\frac{A_r^*}{3} \right)^{3/4} \ln \left[\frac{A_r^*}{3a_c^*} \right] + \frac{3K\phi}{4} \left(\frac{A_r^*}{3} \right)^{3/4} a_c^{*(1/4)} \tag{6}$$

When $a_l < a_c$, only plastic deformation occurs on the rough surface; thus:

$$P^* = K\phi A_r^* \tag{7}$$

The above fundamental formulas of the MB fractal contact theory characterize the real contact area and contact load of two contacting surfaces at different deformation stages (elastic and plastic) by introducing the fractal dimension and scale coefficient, establishing key theoretical support for the subsequent construction of an equivalent friction coefficient model.

2.2 Friction Force Model Considering Adhesion Theory and Plowing Effect

A fundamental point in the simple adhesion friction theory proposed by Bowden et al. (1945) [8] is that the friction force is the sum of the resistances generated by the adhesion effect and the plowing effect. The adhesion effect refers to the strong interaction between atoms and molecules at local real contact points of two solid surfaces due to sufficiently close distance and high local pressure, which requires shearing these bonds during relative sliding. This shear resistance paid to break the interfacial bonds is the adhesive component of the friction force. The plowing effect refers to the harder asperities of the friction pair being "pressed into" the softer counterpart surface under normal load; when relative sliding occurs, these hard asperities act as miniature "plows". Instead of sliding along the soft material surface, they remain embedded within the soft material, forcibly squeezing, bulging, and pushing the soft material ahead to the sides during friction, thereby forming microscopic grooves. Assuming the asperities are conical, the contact area of the friction pair consists of two parts: the fitting area between the hard asperity and the soft material groove (which is the area of the adhesion effect), and the end face (which is the area of the plowing effect), where the hard peak pushes the soft material during sliding. Therefore, the composition of the friction force F_f is given by Eq. (8):

$$F_f = T + P_e = A_r \tau_b + S\sigma_y \tag{8}$$

where T is the shear force, P_e is the plowing force, τ_b is the shear strength, and S is the end face area where the plowing effect occurs.

Assuming the asperities on the hard material surface consist of many cones with a semi-angle θ, as shown in Fig.(1). Under normal load, the hard peaks embed into the soft material to a depth h. During sliding friction, only the front surface of the cones contacts the soft material. The projected area of the contact surface on the horizontal plane is $A = \pi d^2 / 8$, and the projected area on the vertical plane is $S = dh / 2$. Thus, the relationship between the normal projected area and the end face can be expressed as Eq. (9):

$$\frac{S}{A} = \frac{2}{\pi} \cot\theta \tag{9}$$

Therefore, the friction force expression (8) can be further derived as Eq. (10):

ISSN: 2414-1895 DOI: 10.6919/ICJE.202611_12(11).0012

$$F_f = T + P_e = A_r \tau_b + \frac{2}{\pi} \cot\theta A_{rp} \sigma_y \tag{10}$$

In summary, the friction force expression considering the adhesion theory and plowing effect is established. The total contact area and plastic contact area in this expression can be calculated using the MB fractal contact theory. Then, the required friction coefficient can be obtained from the classical tribological law $F_f = \mu P$.

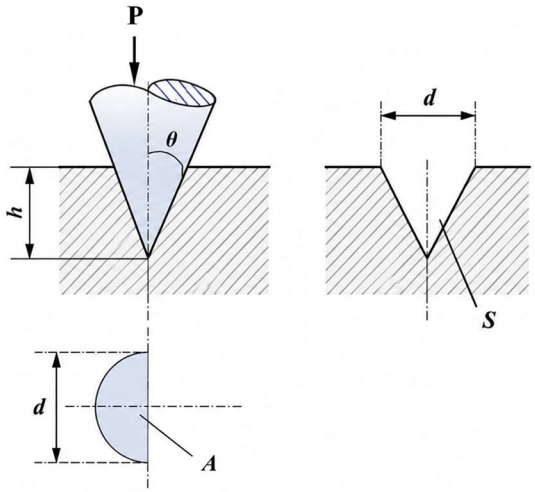


Fig. 1 Schematic diagram of asperity embedding into soft material

2.3 Determination and Calculation of Fractal Dimension and Roughness Amplitude

There are various methods for determining the fractal dimension [9], including the divider method, box-counting method, variogram method, structure function method, and power spectrum method. This paper adopts the power spectrum method to extract the fractal dimension of the spline tooth surface profile. The power spectrum method uses the power spectrum *S(f)* as a measure and the frequency *f* as a scale parameter. According to fractal theory, the power spectral density of an ideal fractal surface exhibits power-law decay with increasing frequency, yielding:

$$S(f) \propto f^{-(5-2D)} \tag{11}$$

In practical applications, the power spectrum curve is obtained by performing a Fast Fourier Transform (FFT) on the discrete signals of the surface profile. In a double-logarithmic coordinate system, linear fitting of the measured data yields the slope α of the fitted line, leading to the logarithmic form of Eq. (12):

$$\lg S(f) = -(5-2D)\lg f + C \tag{12}$$

Thus, the relationship between the slope α and the exponent term is:

$$\alpha = -(5-2D) \tag{13}$$

From this, the fractal dimension of the profile curve can be derived:

ISSN: 2414-1895 DOI: 10.6919/ICJE.202611_12(11).0012

$$D = \frac{5+\alpha}{2} \tag{14}$$

The roughness amplitude G^* is determined according to the study in Ref. [9]:

$$G^* = 10^{-\frac{5.26}{Ra^{0.042}}} \tag{15}$$

where R_a represents the roughness.

3. Experimental Design

3.1 Specimen Preparation

To verify the rationality of the theoretical model and obtain the actual friction coefficient parameters of the spline specimens, three groups of spline pairs (A, B, and C) were selected as the research objects (Fig.2). The three pairs of specimens were all from the same production batch, adopting identical materials, heat treatment processes, and precision grinding machining flows, ensuring high consistency in their macroscopic geometric dimensions and microscopic surface morphological characteristics. The introduction of three parallel specimens aims to eliminate errors caused by the contingency of a single sample through multi-sample statistical analysis, and to verify the stability of the MB fractal friction model. The parameters of the spline specimens are shown in Table 1.



Fig. 2 Spline specimens

Table 1. Parameters of spline specimens

Parameter	Value
Tooth number N	15
Module (mm)	1.25
Pressure angle (°)	30
Tooth width L (mm)	10
Material	9310

During machining, storage, and transportation, spline tooth surfaces readily adsorb cutting fluid residues, oil stains, and tiny metal chips. If observed directly, these foreign attachments not only obscure the true microscopic surface texture but also produce diffuse reflection or spurious signals under an optical microscope, leading to distortion in the extraction of the fractal dimension. To eliminate the interference of tooth-surface attachments with microscopic morphology observation and fractal parameter calculation, the three groups of spline pairs were cleaned before observation using a KQ-350DE desktop numerically controlled ultrasonic cleaner (Fig. 3).

ISSN: 2414-1895 DOI: 10.6919/ICJE.202611_12(11).0012



Fig. 3 KQ-350DE desktop numerically controlled ultrasonic cleaner

3.2 Surface Morphology Observation

The three-dimensional surface morphology of the spline specimens was observed using an optical digital microscope (OLYMPUS DSX510) (Fig. 4). This equipment mainly relies on optical imaging combined with computer software for analysis. In terms of hardware, the microscope body uses high-precision lenses and a lighting system to acquire tooth-surface images; in terms of software, by controlling the optical parameters and employing depth-of-field synthesis technology, the acquired multi-layer images are stacked and ultimately stitched into a complete three-dimensional morphology map, thereby obtaining the fine features of the tooth surface.



Fig. 4 OLYMPUS DSX510 optical digital microscope

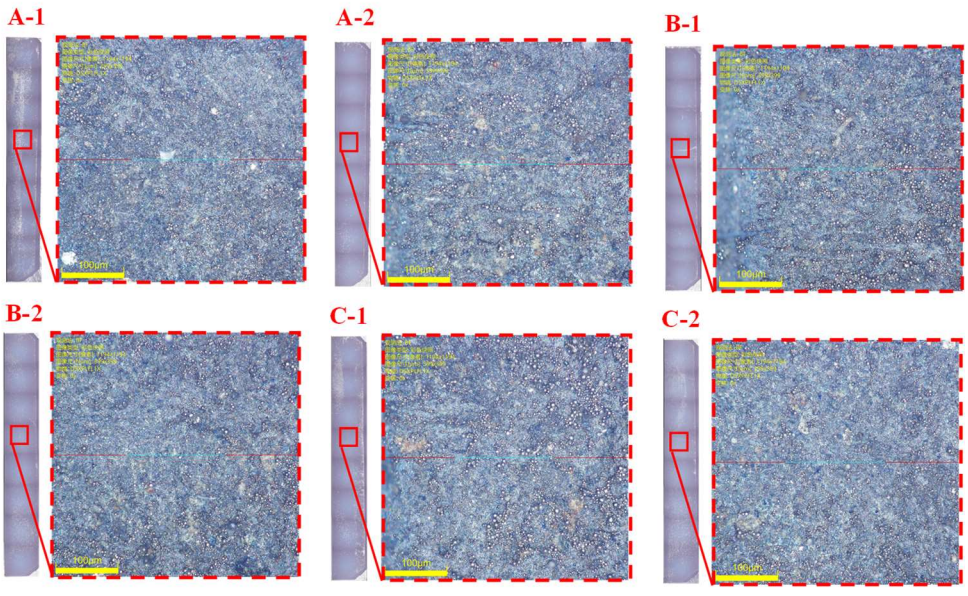


Fig. 5 Microscopic surface morphology images of spline specimens

ISSN: 2414-1895 DOI: 10.6919/ICJE.202611_12(11).0012

Using the aforementioned experimental instruments, tooth-surface observations were conducted on the three groups of spline specimens (*A*, *B*, and *C*). To ensure sample randomness, two tooth surfaces were randomly selected from each group for measurement. The corresponding three-dimensional morphology maps were sequentially numbered as *A-1* and *A-2*, *B-1* and *B-2*, and *C-1* and *C-2*, with the observation results shown in Fig.5.

To facilitate the subsequent extraction and calculation of roughness and fractal dimension, one-dimensional profile curves *z(x)* were extracted from the three-dimensional morphology maps, with three profile curves randomly selected from each map. The 18 extracted one-dimensional profile curves were plotted as area-filled graphs, as shown in Figs. 6–8. In these graphs, the horizontal axis represents the sampling displacement along the tooth-surface normal direction, and the vertical axis represents the height relative to the reference plane. By observing the density of curve fluctuations and their amplitudes, the roughness of different tooth-surface regions can be qualitatively compared. These curves are strictly numbered according to the specimen source and sampling location, sequentially as *A-1(1), A-1(2), A-1(3), A-2(1), …, C-2(3)*, ensuring the traceability of the data sources and providing reliable input data for the subsequent power spectrum analysis.

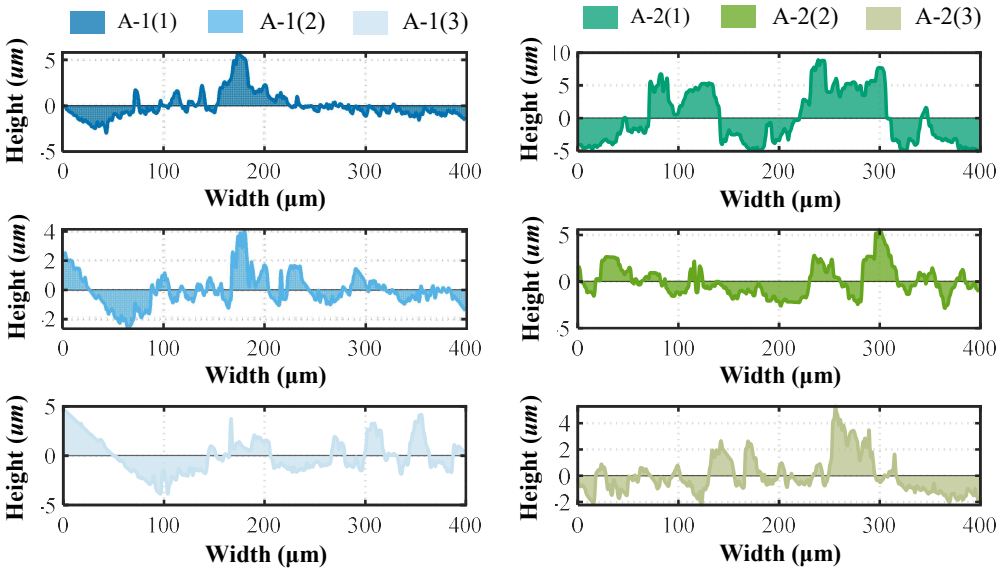


Fig.6 Area-filled graphs of one-dimensional profiles (sampling locations: *A-1* and *A-2*)

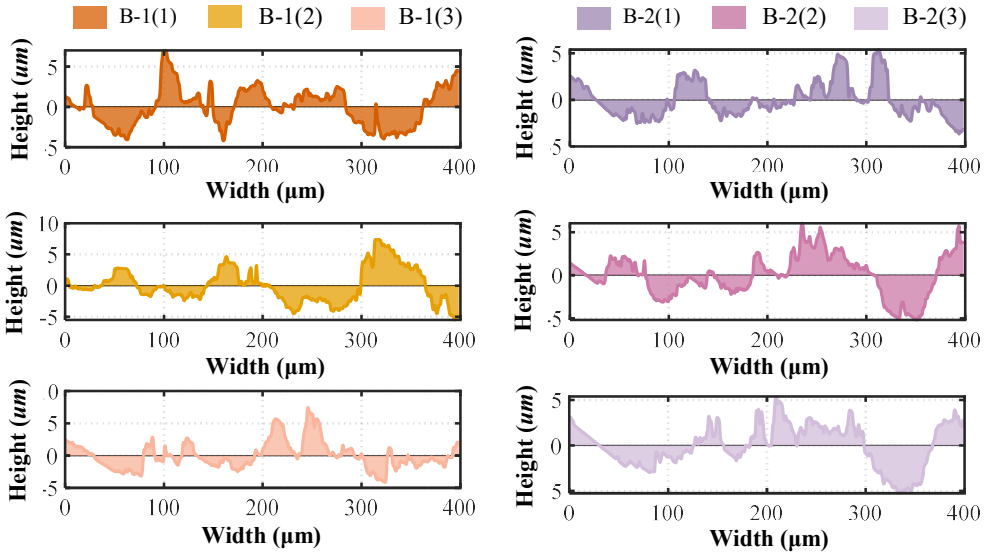


Fig. 7 Area-filled graphs of one-dimensional profiles (sampling locations: *B-1* and *B-2*)

ISSN: 2414-1895 DOI: 10.6919/ICJE.202611_12(11).0012

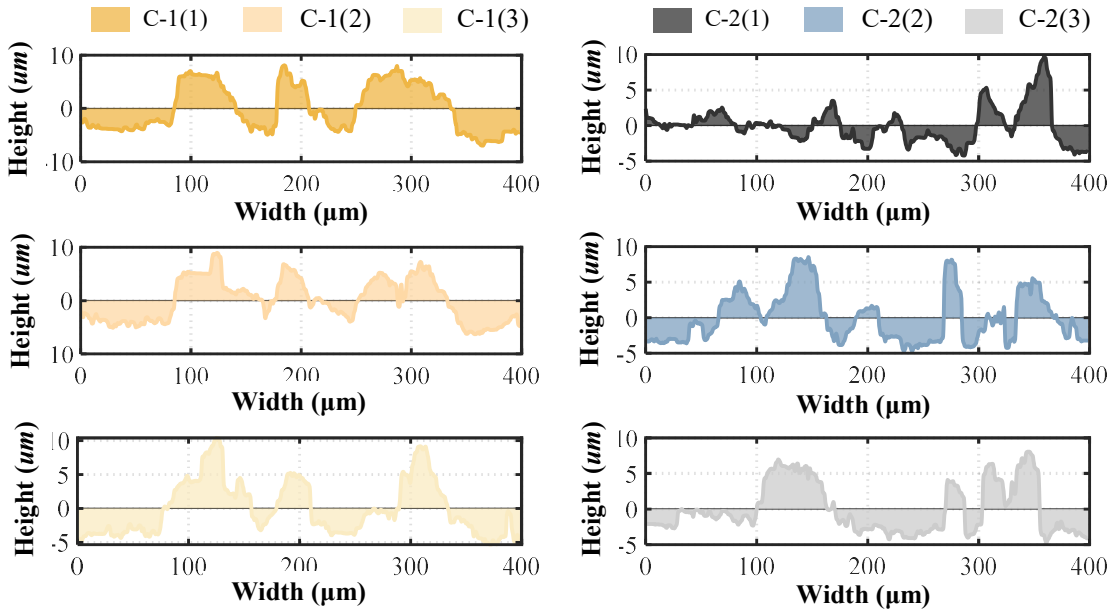


Fig. 8 Area-filled graphs of one-dimensional profiles (sampling locations: *C-1* and *C-2*)

4. Results and Discussion

4.1 Surface Morphology Characteristics and Roughness

Figs. 6–8 show the area-filled graphs of 18 one-dimensional profile curves from 6 sampling regions. The roughness Ra of each profile curve is listed in Table 2.

Table 2. Roughness values

No.	$Ra(\mu m)$	No.	$Ra(\mu m)$
A-1(1)	1.440	B-2(1)	1.924
A-1(2)	1.106	B-2(2)	2.419
A-1(3)	1.801	B-2(3)	2.382
A-2(1)	4.089	C-1(1)	4.471
A-2(2)	1.645	C-1(2)	4.049
A-2(3)	1.412	C-1(3)	4.075
B-1(1)	2.369	C-2(1)	2.567
B-1(2)	2.765	C-2(2)	3.532
B-1(3)	2.169	C-2(3)	3.546

As can be seen from Table 2, the roughness R_a of the 18 profile curves ranges from 1.106 to 4.471 μm, showing significant differences among different sampling regions. The surface of group *A* specimens is relatively smooth, with most profiles having R_a below 2 μm ;group *B* specimens show R_a concentrated between 2 and 3 μm ; group C specimens exhibit the roughest surface, with some profiles exceeding 4 μm . Significant variations in R_a are also observed across different tooth surfaces of the same specimen and different positions on the same tooth surface, reflecting the randomness and non-uniformity of the precision grinding surface morphology. This phenomenon indicates that a single R_a value cannot comprehensively characterize the microscopic morphology of the tooth surface, making it necessary to introduce fractal parameters for a more refined description of the surface.

ISSN: 2414-1895 DOI: 10.6919/ICJE.202611_12(11).0012

4.2 Extraction of Fractal Parameters and Calculation of Friction Coefficient

The fractal dimension of each sampling region was determined using the power spectrum method. The double-logarithmic plots of the one-dimensional power spectral density of the surface profiles in each region are shown in Figs. 9–14.

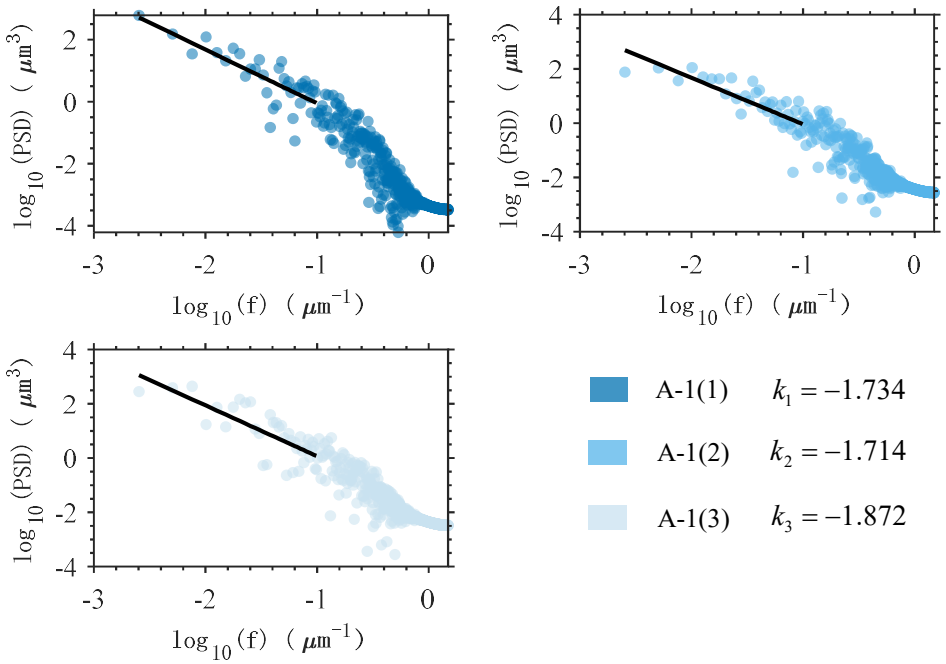


Fig. 9 Double-logarithmic plots of one-dimensional power spectral density (sampling location: *A-1*)

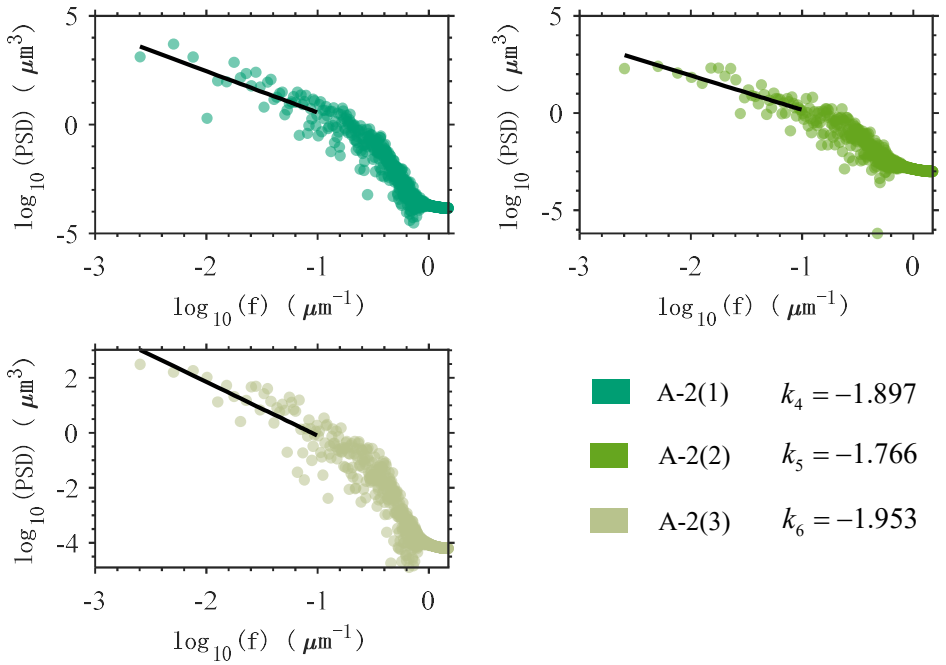


Fig. 10 Double-logarithmic plots of one-dimensional power spectral density (sampling location: *A-2*)

ISSN: 2414-1895 DOI: 10.6919/ICJE.202611_12(11).0012

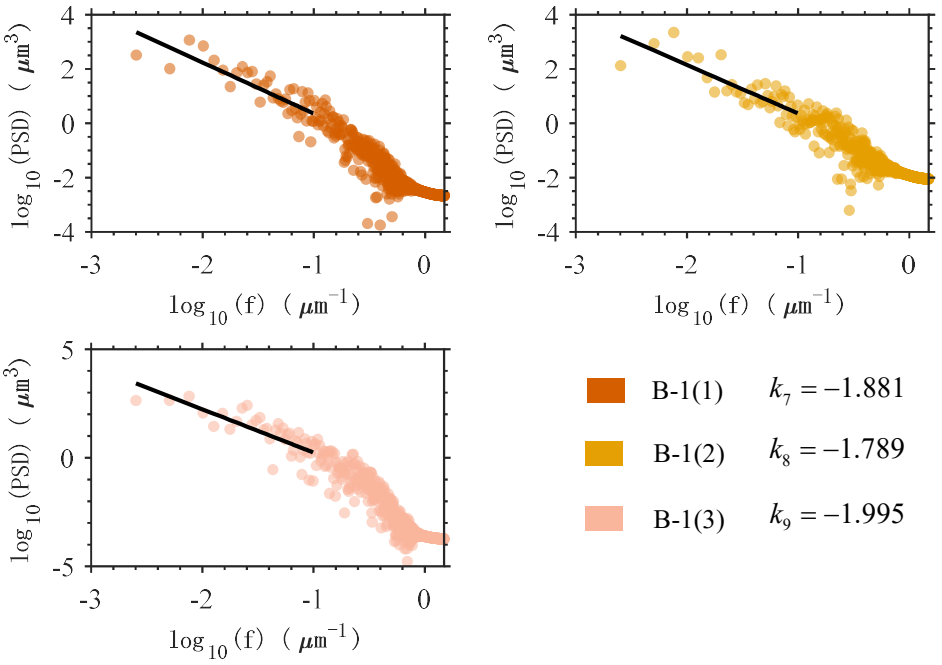


Fig. 11 Double-logarithmic plots of one-dimensional power spectral density (sampling location: *B-1*)

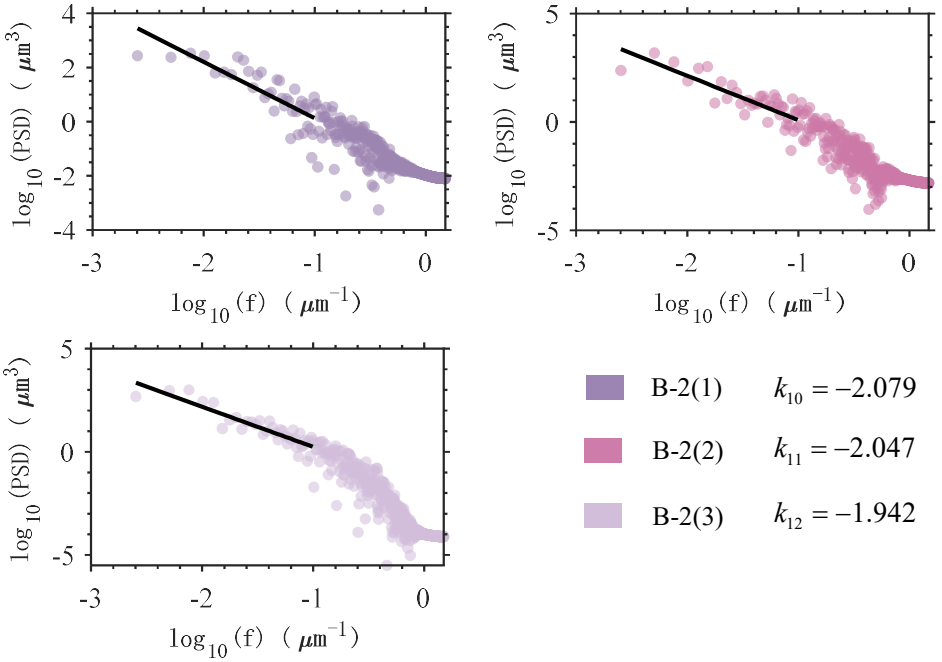


Fig. 12 Double-logarithmic plots of one-dimensional power spectral density (sampling location: *B-2*)

ISSN: 2414-1895 DOI: 10.6919/ICJE.202611_12(11).0012

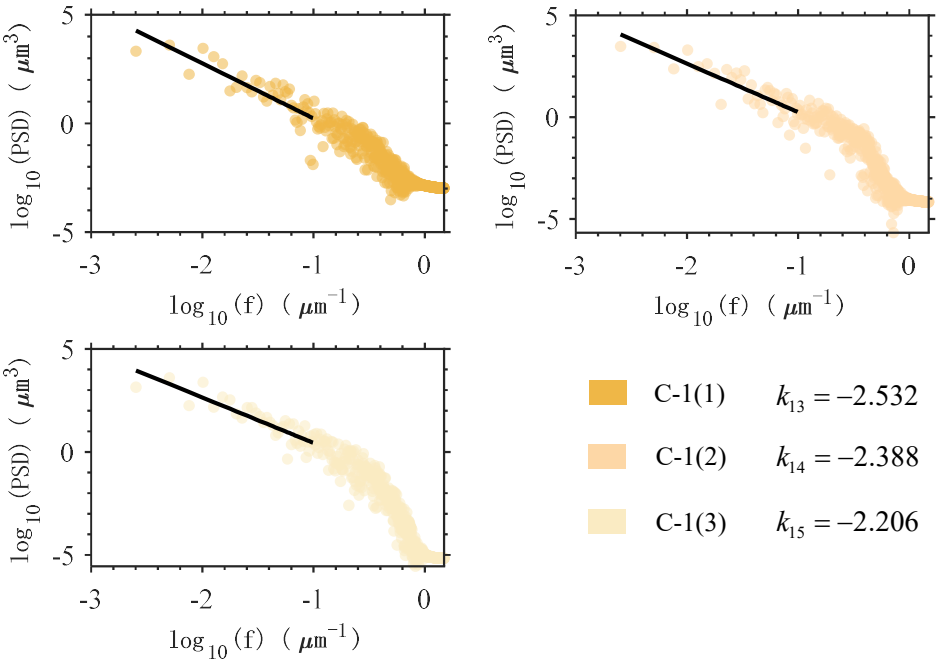


Fig. 13 Double-logarithmic plots of one-dimensional power spectral density (sampling location: *C-1*)

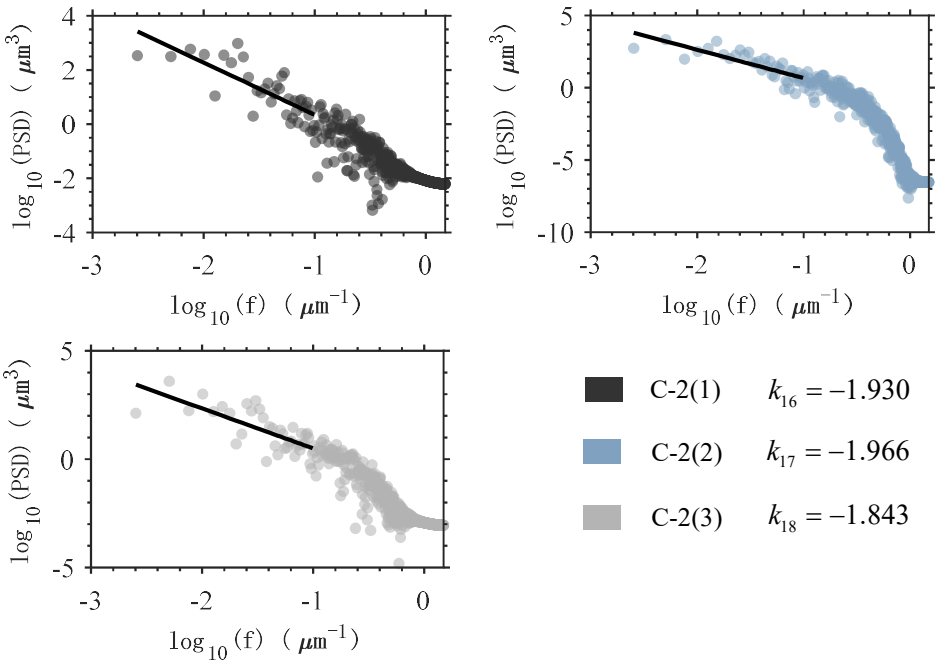


Fig. 14 Double-logarithmic plots of one-dimensional power spectral density (sampling location: *C-2*)

Fig.9 shows the double-logarithmic power spectral density plots of the three profile curves in sampling area *A-1*, with regression line slopes of k_1=-1.734, k_2=-1.714, and k_3=-1.872. Fig.10 shows the double-logarithmic power spectral density plots for sampling area *A-2*, with slopes of k_4=-1.897, k_5=-1.766, and k_6=-1.953. Fig.11 shows the plots for area *B-1*, with slopes of k_7=-1.881, k_8=-1.789, and k_9=-1.995. Fig.12 shows the plots for area *B-2*, with slopes of k_{10}=-2.079, k_{11}=-2.047, and k_{12}=-1.942. Fig.13 shows the plots for area *C-1*, with slopes of k_{13}=-2.532, k_{14}=-2.388, and k_{15}=-2.206. Fig.14 shows the plots for area *C-2*, with slopes of k_{16}=-1.930, k_{17}=-1.966, and k_{18}=-1.843.

ISSN: 2414-1895 DOI: 10.6919/ICJE.202611_12(11).0012

The fractal dimension D of each profile curve is calculated using Eq. (14), and the roughness amplitude G^* is calculated using Eq. (15) combined with the roughness Ra. These are substituted into the friction coefficient model established in Sections 2.1 and 2.2 for numerical solution, and the results are summarized in Table 3.

Table 3. Fractal dimension, roughness amplitude, and friction coefficient

No.	D	G^*	μ
A-1(1)	1.633	$6.605e^{-6}$	0.07
A-1(2)	1.643	$5.783e^{-6}$	0.07
A-1(3)	1.564	$7.385e^{-6}$	0.13
A-2(1)	1.557	$1.102e^{-5}$	0.13
A-2(2)	1.617	$7.061e^{-6}$	0.08
A-2(3)	1.524	$6.542e^{-6}$	0.17
B-1(1)	1.560	$8.455e^{-6}$	0.13
B-1(2)	1.606	$9.119e^{-6}$	0.09
B-1(3)	1.503	$8.096e^{-6}$	0.19
B-2(1)	1.461	$7.631e^{-6}$	0.24
B-2(2)	1.477	$8.542e^{-6}$	0.22
B-2(3)	1.530	$8.476e^{-6}$	0.16
C-1(1)	1.234	$1.150e^{-5}$	0.21
C-1(2)	1.306	$1.097e^{-5}$	0.24
C-1(3)	1.398	$1.100e^{-5}$	0.25
C-2(1)	1.535	$8.794e^{-6}$	0.15
C-2(2)	1.517	$1.027e^{-5}$	0.17
C-2(3)	1.579	$1.029e^{-5}$	0.11

As can be seen from Table 3, the fractal dimension D of the 18 profile curves ranges from 1.234 to 1.643, the roughness amplitude G^* ranges from 5.783×10^{-6} to 1.150×10^{-5}, and the calculated friction coefficient μ ranges from 0.07 to 0.25.

4.3 Relationship between Friction Coefficient and Fractal Parameters

As observed from the data in Table 3, there is a certain correlation trend between the friction coefficient μ and the fractal dimension D. When D is relatively large (approximately above 1.6), μ is relatively low (0.07–0.13); when D is small (1.2–1.4), μ is relatively high (0.21–0.25). This trend aligns with the physical expectations of fractal contact theory: the fractal dimension D reflects the complexity of the surface profile and its space-filling capacity. A smaller D implies stronger irregularity of the surface profile at the microscopic scale, sharper micro-asperities, and a more significant plowing effect, thereby leading to an increase in the friction coefficient.

The influence of the roughness amplitude G^* on the friction coefficient is relatively complex. G^* reflects the amplitude characteristics of surface roughness, and a larger G^* indicates greater surface amplitude fluctuation. As shown in Table 3, the G^* of the Group C specimens is generally higher (approximately 1.1×10^{-5}), corresponding to a higher friction coefficient (0.21–0.25), which is consistent with the distribution pattern of roughness Ra.

ISSN: 2414-1895 DOI: 10.6919/ICJE.202611_12(11).0012

4.4 Comparison and Verification with Traditional Empirical Values

The empirical values of the surface friction coefficient for traditional gear tooth machining processes usually range from 0.05 to 0.3. The friction coefficients obtained in this paper range from 0.07 to 0.25, fully falling within this empirical interval, which verifies the rationality and effectiveness of the established MB fractal friction model for extracting the friction coefficient of spline tooth surfaces.

Meanwhile, the results of this paper also reveal the shortcomings of the traditional empirical value method: for spline specimens from the same batch and processed with the same technology, the friction coefficient at different tooth surface positions fluctuates between 0.07 and 0.25, with differences reaching more than 3 times. If a fixed empirical value is taken in the rotor dynamics model, it will fail to reflect the friction characteristic variations caused by surface topography differences, potentially leading to deviations in dynamics prediction. By extracting fractal parameters from measured tooth surface topographies, the method proposed in this paper can provide a more accurate equivalent friction coefficient for dynamics models.

4.5 Applicability and Limitations of the Model

It should be noted that the extraction of the friction coefficient in this paper is based on the following assumptions: (1) the asperity shape is simplified as a cone; (2) the effects of lubricant and temperature on friction behavior are neglected; (3) the material parameters are taken as static values, without considering the strain rate effect. Therefore, the results of this paper are applicable to the estimation of the friction coefficient under dry friction or boundary lubrication conditions. For fully oil-lubricated or high-temperature working conditions, the model needs to be extended by introducing parameters related to lubricant film thickness and temperature.

In addition, no pin-on-disc friction test was conducted in this paper to directly verify the model results experimentally; instead, indirect verification was performed by comparison with empirical values from the literature. Future work may consider carrying out friction tests on specimens of the same material and process to further verify the prediction accuracy of the model.

5. Conclusion

This paper relies on the MB fractal contact theory, incorporates the adhesion and plowing effects into a unified analysis framework, establishes an analytical model between the friction coefficient of spline tooth surfaces and fractal parameters, and extracts actual tooth surface fractal parameters through ultra-depth-of-field optical microscopy observation and the power spectrum method, completing the numerical solution of the friction coefficient. The main conclusions are as follows:

(1) An MB fractal friction model considering adhesion and plowing effects is constructed, realizing the quantitative mapping between the friction coefficient μ and the fractal dimension D and roughness amplitude G^*, providing a theoretical approach for determining the friction coefficient with surface topography effects included.

(2) Ultra-depth-of-field optical microscopy is used to observe the topography of 6 tooth surface areas of three groups of spline specimens, intercepting 18 one-dimensional profile curves. The fractal dimension D extracted by the power spectrum method ranges from 1.234 to 1.643, and the roughness amplitude G^* ranges from 5.783×10^{-6}–1.150×10^{-5}.

(3) The friction coefficient μ obtained from the model calculation ranges from 0.07 to 0.25, showing good agreement with the traditional ground tooth surface empirical interval (0.05–0.3). The smaller the fractal dimension, the stronger the microscopic surface irregularity, the more significant the plowing effect, and the larger the friction coefficient.

(4) For spline specimens of the same batch and identical process, the friction coefficient difference at different tooth surface positions can exceed 3 times, indicating that adopting a fixed empirical value cannot reflect the influence of surface topography differences on friction characteristics. The proposed method can provide an equivalent friction coefficient accounting for surface topography effects for spline rotor dynamics models.

ISSN: 2414-1895 DOI: 10.6919/ICJE.202611_12(11).0012

References

[1] Ratsimba, C. H. H., McColl, I. R., Williams, E. J., Leen, S. B., & Soh, H. P. (2004). Measurement, analysis and prediction of fretting wear damage in a representative aeroengine spline coupling. Wear, 257(11), 1193–1206. https://doi.org/10.1016/j.wear.2004.08.003

[2] Zhao, G., Zhao, X. Y., Qian, L. T., Yuan, Y., Ma, S., & Guo, M. (2022). A review of aviation spline research. Lubricants, 11(1), Article 6. https://doi.org/10.3390/lubricants11010006

[3] Beam, A. S. (1959). The advantages of involute spline and serrations from a gaging standpoint. SAE Technical Paper, 590200. https://doi.org/10.4271/590200

[4] Majumdar, A., & Bhushan, B. (1991). Fractal model of elastic-plastic contact between rough surfaces. Journal of Tribology, 113(1), 1–11. https://doi.org/10.1115/1.2920588

[5] Majumdar, A., & Tien, C. L. (1990). Fractal characterization and simulation of rough surfaces. Wear, 136(2), 313–327. https://doi.org/10.1016/0043-1648(90)90154-3

[6] Warren, T. L., & Krajcinovic, D. (1996). Random cantor set models for the elastic-perfectly plastic contact of rough surfaces. Wear, 196(1–2), 1–15. https://doi.org/10.1016/0043-1648(95)06785-X

[7] Majumdar, A., & Bhushan, B. (1991). Fractal model of elastic-plastic contact between rough surfaces. Journal of Tribology, 113(1), 1–11. https://doi.org/10.1115/1.2920588

[8] Bowden, F. P., & Tabor, D. (1964). The friction and lubrication of solids. Clarendon Press.

[9] Ge, S. R., & Zhu, H. (2005). Fractal theory of tribology. China Machine Press.